Dalton Transactions

ROYAL SOCIETY OF CHEMISTRY

PAPER

View Article Online
View Journal | View Issue

Cite this: *Dalton Trans.*, 2024, **53**, 4705

Neutral 2-phenylbenzimidazole-based iridium(III) complexes with picolinate ancillary ligand: tuning the emission properties by manipulating the substituent on the benzimidazole ring†

Emiliano Martínez-Vollbert, [a] Christian Philouze,[a] Théo Cavignac, [b] ‡ Camille Latouche, *[b,c] Frédérique Loiseau*[a] and Pierre-Henri Lanoë *[a]

Received 20th October 2023,
Accepted 15th December 2023

DOI: 10.1039/d3dt03498d

rsc.li/dalton

We report the synthesis and characterization of ten neutral bisheteroleptic iridium(III) complexes with 2-phenylbenzimidazole cyclometallating ligand and picolinate as ancillary ligand. The 2-phenylbenzimidazole has been modified by selected substituents introduced on the cyclometallating ring and/or on the benzimidazole moiety. The integrity of the complexes has been assessed by NMR spectroscopy, by high-resolution mass spectrometry and by elemental analysis. The complexes are demonstrated to be highly phosphorescent at room temperature and a luminescence study with comprehensive *ab initio* calculations allow us to determine the lowest emitting excited state which depends on the substituent nature and its position on the cyclometallating ligand.

Introduction

Organic light-emitting diodes (OLEDs) and light-emitting electrochemical cells represent very interesting technologies for lighting displays as such devices are able to work at low voltage.[1–3] In these technologies, the excitons generated by the recombination of injected holes and electrons are in both singlet and triplet excited states, with a ratio of 1 : 3, making the theoretical external quantum efficiency (EQE) of only 25% for pure organic devices that can emit solely from the singlet excited state. The seminal work of Thompson and Forrest has demonstrated that phosphorescent emitters are able to convert a singlet exciton to a triplet one, therefore offering the possibility to harvest 100% of the exciton and raise the theoretical EQE to unity.[4–6] Thus, since the early 2000s the search for highly emissive and color-tunable transition metal-based emitters has shown an impressive boom. Among the transition metal complexes, two metals display excellent potentials in lighting displays with complexes displaying very high quantum yields, relatively short lifetimes and high emission energy tunability, these being octahedral Ir(III) and square planar Pt(II).[7] Those emission properties have been brought to light thanks to cyclometallation. Indeed, the metal–carbon bond with the strong σ donor ability from C^-, along with the π-acceptor ability of pyridine, gives a very strong ligand field to these metals, leading to the abovementioned tremendous photophysical properties of the lowest excited state. Consequently, cyclometallated Ir(III) and Pt(II) complexes are studied or used in numerous applications, spanning from triplet emitters in electroluminescent devices,[3,8–13] sensors,[14–18] theragnostic and/or therapeutic agents[19–24] to photosensitizers and photocatalysts[14,25,26] to name a few examples.

Neutral Ir(III) complexes have been particularly studied and can be divided into three main types: tris-homoleptic *fac*/*mer*-Ir(C^N)$_3$, where C is a cyclometallated carbon and N is a heterocyclic nitrogen; bis-heteroleptic Ir(C^N)$_2$(LX), where LX represents an anionic ancillary ligand; and tris-heteroleptic of the form Ir(N^C^N)(C^N)X, where X is an anionic ligand, typically a chloride.[27–30] The emission properties of Ir(III) complexes are often an intriguing interplay of emissive excited states, taking as reference the well-known *fac*-Ir(ppy)$_3$ (hereafter denoted simply Ir(ppy)$_3$, where ppy = 2-phenylpyridine). The lowest-energy absorption is of ^{1}MLCT (metal-to-ligand charge transfer) nature and likewise the emissive level is recognized to be of ^{3}MLCT nature (λ_{em} = 508 nm, τ = 1.6 μs in MeTHF at r.t.).[31,32] Higher-lying excited states of ^{3}IL (intraligand or ligand-centred) nature are also present and in several cases the energy separation with the triplet MLCT excited state

[a]*Univ. Grenoble Alpes, CNRS, DCM, 38000 Grenoble, France. E-mail: frederique.loiseau@univ-grenoble-alpes.fr, pierre-henri.lanoe@univ-grenoble-alpes.fr*
[b]*Université de Nantes, CNRS, Institut des Matériaux Jean Rouxel, IMN, F-44000 Nantes, France. E-mail: camille.latouche@cnrs-imn.fr*
[c]*Insitut universitaire de France (IUF), France*

† Electronic supplementary information (ESI) available. CCDC 2246643–2246645. For ESI and crystallographic data in CIF or other electronic format see DOI: https://doi.org/10.1039/d3dt03498d

‡ Please contact this author regarding the theoretical aspects of the article.

is rather narrow or even "inverted", ^{3}IL being the lowest excited state. This is the case for the heteroleptic complex (thpy)$_2$Ir(acac) (thpy = thienylpyridine, acac = acetylacetonate) displaying an r.t. emission at λ_{em} = 562 nm with τ = 5.3 μs in MeTHF, which is recognized to be a genuine ^{3}IL emitter.[28] In addition, the lowest-lying excited state of bis-heteroleptic Ir(III) complexes can also be the ligand-to-ligand charge transfer (^{3}LL′CT, L′ = ancillary ligands) excited state. The ^{3}CT state radiative deactivation results in a broad emission profile and goes along with a rigidochromism effect at low temperature (hypsochromic shift), while the ^{3}IL radiative deactivation results in a structured emission profile and no rigidochromism is observed and even a bathochromic shift can be observed.[12,33–36] In addition, the nature of the emitting excited states will also affect the radiative constant (k_r), which is typically of the order of 2 × 10^5 s^{-1} when the emission emanates from ^{3}MLCT/^{3}LL′CT excited state and lower in the case of ^{3}IL phosphorescence.[36,37] However, frequently, cyclometallated Ir(III) complexes demonstrate an emission being a mixture of the ^{3}MLCT and ^{3}LC excited states.

The majority of the reported Ir(III) complexes, as for the Pt(II) ones, are derived directly from the introduction of substituent(s) on the 2-phenylpyridine ligand, and their photophysical properties are well established. On the other hand, complexes based on 2-phenylbenzimidazole as cyclometallating ligand represent a smaller family, but are not devoid of interest. Numerous host materials for phosphors are based on benzimidazole heterocycles for OLEDs regarding their good electron mobility with excellent thermal stability.[38–41] From a synthesis point of view, this ligand is an attractive scaffold for cyclometallating ligands, as it presents three divergence points which can be independently modified: the introduction of alkyl or aryl can be performed on the secondary amine, on the phenyl ring or on the benzimidazole ring, and the synthesis does not require the use of palladium-catalysed cross-coupling reactions.[42,43] Fine tuning of the emission properties has been achieved by the introduction of electron withdrawing/donating groups on the cyclometallating arene,[41,44–56] while the modification of the benzimidazole moiety has been performed by ring expansion.[57] For example, the introduction of –OCH$_3$ and CN groups on the cyclometallating phenyl ring allowed tuning of the luminescence from 496 nm to 605 nm with quantum yield from 0.05 to unity.[47] Recently, we focused our effort toward the modification of this moiety by the introduction of chosen substituents leading to highly emissive cationic Ir(III) complexes and the luminescence and electrochemical

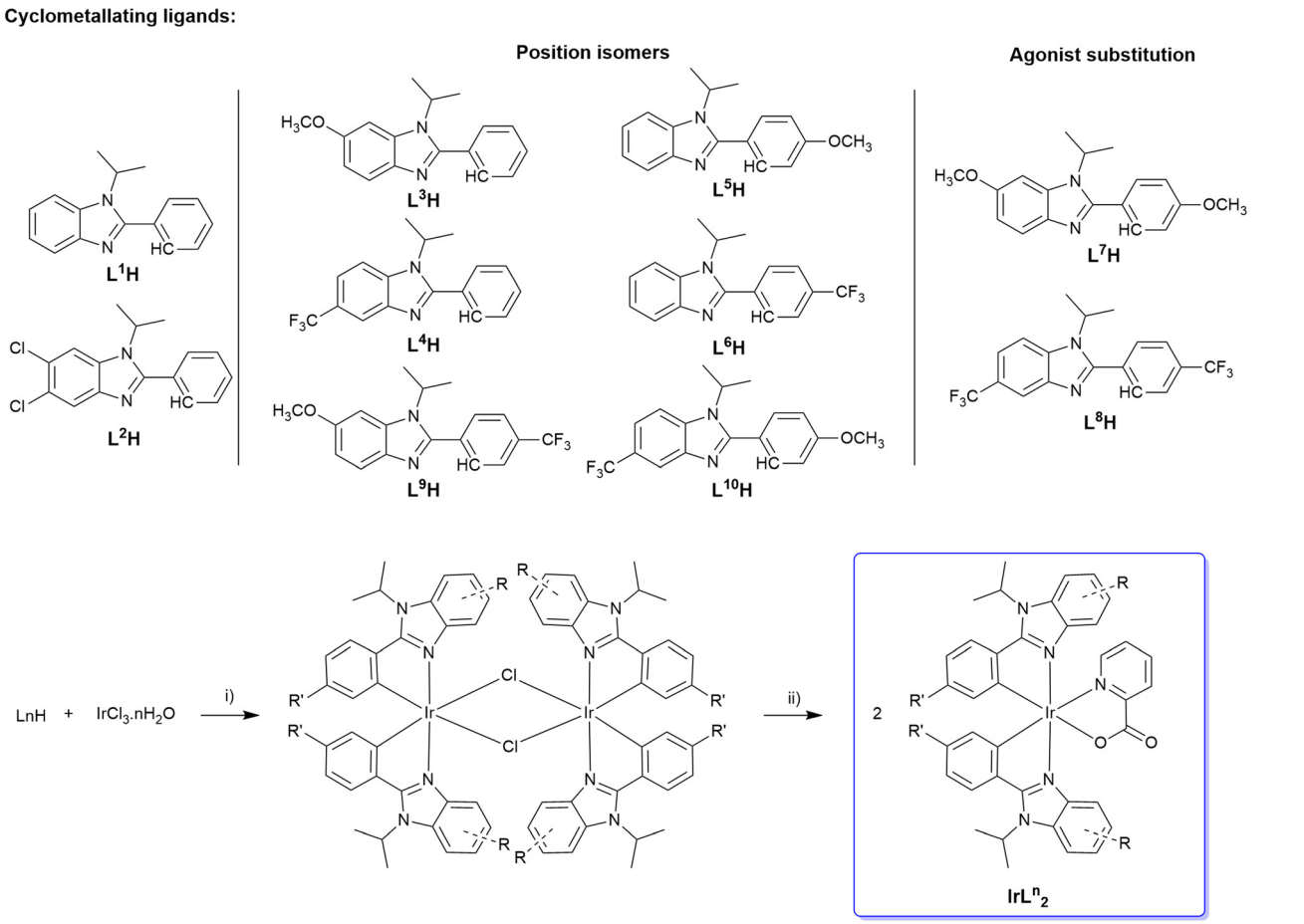

Scheme 1 Top: proligand structures. Bottom: synthesis of the complexes. (i) EtOEtOH/H$_2$O reflux; (ii) 2-picolinic acid, Na$_2$C$_2$O$_3$ 100 °C.

properties have been successfully tuned.[58] In addition, we demonstrated that two complexes had emitting excited state that was sensitive to the solvent polarity and it was possible to switch from ^{3}M/LLCT* to ^{3}LC*. Herein, we report a series of neutral Ir(III) complexes featuring 2-phenylbenzimidazole cyclometallating (N^C) ligand and picolinate as ancillary ligand. The N^C ligands (Scheme 1) are designed to study the influence of the substituents' (Cl, CF_3, and OCH_3) electron withdrawing/donating ability by tailoring their localization on the ligand, on either the phenyl or the benzimidazole or both through the synthesis of position isomers. It must be emphasized that the HOMO is usually localized on the Ir-ph moiety and the LUMO on the benzimidazole moiety.[44,56] The experimental data are successively confronted with state-of-the-art computational methods leading to unambiguous attribution of the emitting exciting state.

Results and discussion

Synthesis and characterization

The cyclometallating ligands (**HL^n**, Scheme 1) and μ-dichloridodimers were synthesized following our previous report.[59] The ten new complexes **IrL$^n_2$** were obtained by reacting an excess of picolinic acid with adequate μ-dichloridodimer in the presence of sodium bicarbonate in a mixture of 2-ethoxyethanol/water at 100 °C overnight. After precipitation by water addition and filtration, the solids were purified by flash column chromatography on silica gel using mixtures of dichloromethane/methanol/triethylamine as eluent. All the complexes were characterized by ^{1}H, ^{13}C and ^{19}F (when applicable) NMR, by HRMS and elemental analysis.

Crystallographic quality single crystals of **IrL$^6_2$**, **IrL$^9_2$** and **IrL$^{10}_2$** have been obtained by slow vapor diffusion of diethyl ether or pentane in a concentrated solution of each complex in dichloromethane. The cell parameters of each complex are summarized in Table S1† and selected bond lengths and angles of the three complexes are presented in Table 1, along with those of complex [Ir(ppy)$_2$pic][60] for comparison purpose. The crystallization space groups and Bravais lattices are monoclinic $P2_1/m$ for **IrL$^6_2$** and **IrL$^9_2$**, and triclinic $P\bar{1}$ for **IrL$^{10}_2$**. Each asymmetric unit displays a single complex: four complexes are present in the unit cell for **IrL$^6_2$** and **IrL$^9_2$** and two in the case of **IrL$^{10}_2$**. As expected, we observed in the lattice the two Δ and Λ isomers which arise from the reaction of the picolinate with the μ-dichlorido-bridged Ir dimer having the D_2 symmetric ΔΔ and ΛΛ racemic mixture, where the two C^N ligands have a *cis*-C,C and *trans*-N,N configuration around the metal center.[61–63] The resulting configuration for the three complexes is the expected *mer*-N3 *cis*-C,C *trans*-N,N within the two Δ and Λ isomers (Fig. 1). The reason for this outcome is due to the Ir–Ir distances being rather small below 4 Å, which leads to important steric hindrance and to the so-called *trans* effect of the Ir–C bonds, which induces preferential labilization of the bonds located in *trans* configuration. It results in the stereochemical positioning of Ir–C and Ir–N bonds *trans* to one another.[27,61] The Ir–C and Ir–N_{C^N} bond lengths displayed by the three complexes are similar, ranging from 1.995 to 2.020 Å, and so are the bond angles around the Ir core. The *trans* effect emanating from the strong σ-donating ability of the cyclometallating carbon affects the Ir–N_{pic} bond lengths.[34] The latter are roughly 2.13 Å for the three structures, much longer than the other Ir–N_{C^N} lengths which are of the order of 2.04 Å. The bite angles of both cyclometallating ligand and ancillary ligand are similar through the series and comparable with that of [Ir(ppy)$_2$pic]; the bite angles of ppy ligand and 2-phenylbenzimidazole are around 80°.[60] The C–Ir–C′ angles are about 90.5° for the three complexes, of the same order as the one encountered in [Ir(ppy)$_2$pic] (88.7°). Brought together, the different parameters are coherent with the expected octahedral coordination geometry, with slight distortions of the ligands caused by the formation of the five-membered metallacycles.[34,64–67] A particularity observed for the three complexes is the strong interaction between the hydrogen

Table 1 Some relevant bonding and angle parameters for complexes **IrL$^6_2$pic**, **IrL$^9_2$pic** and **IrL$^{10}_2$pic** along with [Ir(ppy)2(pic)][60] for comparison purpose

Complex	[Ir(ppy)$_2$(pic)]60	IrL$^6_2$	IrL$^9_2$	IrL$^{10}_2$
Ir–C (Å)	2.003(6), 2.012(5)	1.995(5), 2.020(5)	2.003(5), 2.006(5)	1.995(2), 2.009(2)
Ir–NC^N (Å)	2.041(5), 2.052(5)	2.043(3), 2.049(3) 2.031(3), 2.037(3)	2.031(3), 2.037(3)	2.028(2), 2.031(2)
Ir–NN^O (Å)	2.141(5)	2.130(3)	2.121(3)	2.134(2)
Ir–ON^O (Å)	2.156(4)	2.147(3)	2.151(3)	2.157(2)
C–Ir–C′ (°)	88.7(2)	90.5(2)	91.7(2)	89.37(8)
NC^N–Ir–NC^N (°)	175.7(2)	172.6(1)	172.5(1)	173.56(8)
CγC^N–Ir–ON^O (°)	95.4(2)	94.8(2)	93.5(2)	97.93(7)
CδC^N–Ir–NN^O (°)	100.1(2)	97.8(2)	97.8(2)	96.01(7)
N^O bite angle (°)	77.1(2)	76.9(1)	77.1(1)	76.81(6)
C^N bite angle (°)	80.1(2), 81.3(2)	79.2(2), 79.6(2)	79.6(2), 79.6(2)	79.14(7), 79.62(7)
Distortion C^N (°)	2.60, 5.71	15.18, 17.30	12.34, 12.90	8.95, 10.45
Distortion N^O (°)	4.54	6.74	3.60	4.40
H30–H19 H3–H14 (Å)	—	2.055 2.025	2.048, 1.957	1.943, 1.913

Distortion C^N is defined by the angle between the mean planes of the benzimidazole moiety and the phenyl and distortion N^O (picolinato ligand) by the angle of the mean planes of the COO function and the corresponding pyridine.

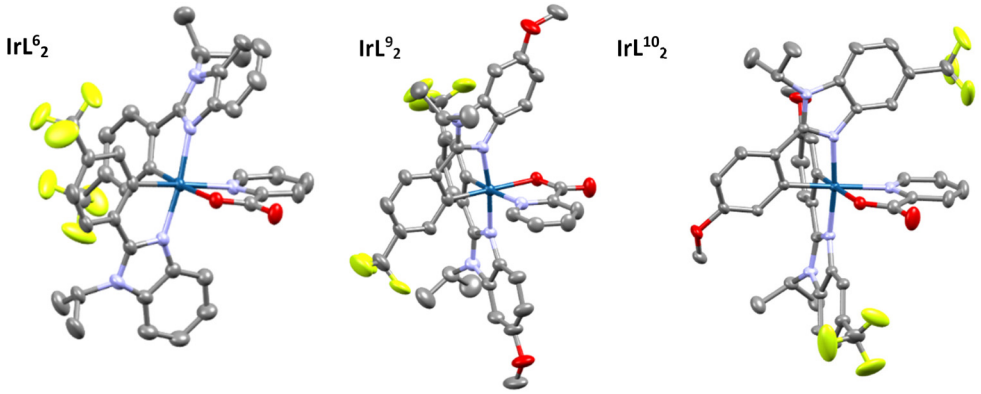

Fig. 1 X-ray molecular structure of complexes **IrL$^6_2$**, **IrL$^9_2$** and **IrL$^{10}_2$**. Thermal ellipsoids are plotted at the 50% probability level. H atoms and solvent molecules are omitted for clarity.

atoms from CH_3CHCH_3 and the *ortho* H from the benzimidazole ring: these two atoms display a distance very inferior to 2.29 Å corresponding to the sum of the van der Waals radii (vdW), ranging from 1.913 Å to 2.055 Å. These strong interactions have been observed before in a cationic series of iridium complexes,[59] and they could be the origin of the strong distortions observed in the cyclometallating ligand (~13°), larger than the ones observed in [Ir(ppy)$_2$pic] (~4°). It is worth noting that these interactions are also observed in solution at room temperature, notably on the ^{1}H NMR spectrum, as the iso-propyl's methyl groups are not equivalent, even at higher temperature, and the central H is observed at lower field than the expected chemical shift (3–4.5 ppm) in all the complexes, with multiplets appearing between 5.8 ppm and 5.56 ppm.

One can notice that the crystal packings of the three complexes display several hydrogen bonds between adjacent complex molecules, involving the oxygen atoms of the picolinate ligand and with distances ranging from 2.397 to 2.679 Å that are inferior to the vdW sum ($\sum_{vdW}(H_{Ar}–O)$ = 2.61 Å and $\sum_{vdW}(H_{Al}–O)$ = 2.72 Å). Other hydrogen bonds are present involving fluorine atoms from the CF_3 group and H···π interactions are also present. These interactions are characterized considering the distances H–X that are inferior to the vdW sum ($\sum_{vdW}(H_{Ar}–C_{Ar})$ = 2.79 Å, $\sum_{vdW}(H_{Ar}–F)$ = 2.56 Å, $\sum_{vdW}(H_{Al}–F)$ = 2.67 Å, and $\sum_{vdW}(H_{Al}–C_{Ar})$ = 2.90 Å). The supramolecular bonds seem to be mainly driven by electrostatic interaction, with the exception of the abovementioned interaction between H30 and H19 that is due to structural hindrance.[68,69]

From a computational point of view, the relaxed ground state structures are in very good agreement with respect to experiment. For instance, for complex **IrL$^6_2$**, the averaged Ir–C and Ir–NC^N computed (experimental) values are 2.002 (2.019) and 2.051 (2.039) Å. Also, the Ir–NN^O and Ir–O–N^O are simulated at 2.150 and 2.171 Å matching well the observed ones using XRD (2.130 and 2.147 Å). These results gave us confidence for the rationalization of the ground and excited state optoelectronic properties.

The electrochemical properties of the complexes have been studied by cyclic voltammetry (CV) in a deaerated 10^{-2} M solution of *n*-NBu_4PF_6 in MeCN as supporting electrolyte, using vitreous carbon as working electrode (5 mm) and $Ag/AgNO_3$ (10^{-2} M) as reference electrode at a scan rate of 100 mV s^{-1}. The redox potentials are given *versus* the reference electrode. CV traces are shown in Fig. S1,† and values are gathered in Table 2. In agreement with previous work on similar complexes, the oxidation peaks in the range 0.55–0.94 V are ascribed to the Ir^{III}/Ir^{IV} couple, whereas the reduction affects principally the cyclometallating ligand.[47,70] Complex **IrL$^1_2$** displays E_{red} at −2.38 V and E_{ox} at 0.61 V, whereas the parent complex [Ir(ppy)$_2$pic] has a smaller ΔE_{redox} with E_{red} at −2.27 V and a E_{ox} at 0.66 V.[71] The differences can be explained by the fact that 2-phenylbenzimidazole is more electron rich than 2-phenylpyridine, which leads **IrL$^1_2$** to be more easily oxidized (*i.e.* the metal center is easier to oxidize) and, consequently, more difficult to be reduced. As expected, the electrochemical properties of the complexes are sensitive to the nature of the substituents, on both the benzimidazole and the phenyl moieties. In reduction, most of the complexes display a reversible reduction wave, with the exception of four of the complexes, whose cyclometallating ligands are substituted by chlorine atoms (**IrL$^2_2$**) and by CF_3 group on the phenyl ring (**IrL$^{6,8,9}_2$**). The introduction of electron withdrawing groups (Cl and CF_3) on the benzimidazole moiety shifts the reduction to less nega-

Table 2 Redox potentials of complexes **IrL$^n_2$pic**: *E* (V) *vs.* $Ag/AgNO_3$ (0.01 M) in deaerated CH_3CN

Complex	E_{Red} (V)	E_{Ox} (V)
IrL$^1_2$	−2.38	0.61
IrL$^2_2$	−2.20^{irr}	0.71
IrL$^3_2$	−2.38	0.57
IrL$^4_2$	−2.34	0.70
IrL$^5_2$	−2.38	0.60
IrL$^6_2$	−2.42^{irr}	0.84
IrL$^7_2$	−2.38	0.55
IrL$^8_2$	−2.21^{irr}	0.94
IrL$^9_2$	−2.41^{irr}	0.80
IrL$^{10}_2$	−2.34	0.71

^{irr} denotes irreversible reduction peak.

tive potential (IrL^2_2, E_{red} = −2.20 V and IrL^4_2, E_{red} = −2.34 V) in comparison with IrL^1_2. In contrast, the introduction of electron donating groups (OMe) solely, on either the benzimidazole and/or the phenyl moieties, does not induce a decrease of the reduction potential ($IrL^{3,5,7}_2$, E_{red} = −2.38 V) with respect to IrL^1_2. In the case of the position isomers substituted both by CF_3 and by OMe groups on the cyclometallating ligand, the influence of the electron-donating group prevails on the reduction potential, albeit the reduction peaks of complexes $IrL^{6,9,8}_2$ are irreversible. Such a behaviour has been previously described.[59] In oxidation, all the complexes display a reversible peak whose potential is dependent on the substituent. As expected, the electron withdrawing CF_3 group and chlorine atoms lead to a more positive E_{ox} in comparison with IrL^1_2. The influence is greater when the group is on the phenyl rather than on the benzimidazole. This agrees with the fact that the HOMO is localized on the Ir-phenyl moiety.[47,72,73] Similarly, the electron donating OMe group, both on the benzimidazole and the phenyl, leads to a decrease in E_{ox} (*vs.* IrL^1_2). However, one can notice that the substitution by CF_3 groups on both "sides" of the cyclometallating ligand has a synergetic effect on E_{ox} (IrL^4_2, E_{ox} = 0.70 V; and IrL^8_2, E_{ox} = 0.94 V); the synergy is less effective in the case of OMe (IrL^3_2, E_{ox} = 0.57 V; and IrL^7_2, E_{ox} = 0.55 V) as the potentials with one or two MeO groups are almost identical. The presence of both OMe and CF_3 groups on the cyclometallating ligand demonstrates the prevalence of the electron withdrawing group over the electron donating group, as shown by the E_{ox} of 0.80 V and 0.71 V of IrL^9_2 and IrL^{10}_2, respectively. One should notice that the incorporation of two OMe moieties for the complex IrL^7_2 induces a less positive oxidation potential than for the other complexes. It should be also noticed that, as expected, all complexes possessing such a donating group have a HOMO partly localized on the OMe moiety. The cyclometallating ligand 2-phenylbenzimidazole, used instead of the most encountered 2-phenylpyridine (ppy), has a substantial effect on the electrochemical properties of complexes in comparison with [Ir(ppy)$_2$pic].

Photophysical properties

Absorption spectroscopy. The absorption spectra of the complexes have been registered in dilute solution of CH_2Cl_2 at room temperature. They are displayed in Fig. 2 and data are gathered in Table 3 (individual absorption spectra are presented in Fig. S2†). The intense bands at around 300 nm can be ascribed to ligand-centred (LC) π–π* transitions from the cyclometallating and ancillary ligands. Broad and relatively weak absorption bands observed in the longer wavelength region, over 350 nm, are attributed to the overlap of metal-to-ligand charge transfer (MLCT) and ligand-to-ligand charge transfer (LLCT) and those over roughly 460 nm to direct absorption from singlet ground state to triplet excited state (Fig. S3†), as a consequence of the strong spin orbit coupling effect exerted by the Ir(III) core.[7,26,74–76] For instance, the less intense lowest-lying bands, displayed as weak tails in the absorption spectra, roughly around 430 nm, are ascribed to spin-forbidden triplet transitions. As expected, a focus on the CT absorption band wavelengths evidences the influence of the substituents: for instance, electron withdrawing groups (CF_3 and Cl) induce a hypsochromic shift and, in contrast, the electron donating methoxy group induces a bathochromic shift. It seems that the influence of the substituent on the absorption band energies does not greatly depend on the position on the cyclometallating ligand. To assign the observed absorption bands, TD-DFT computations were conducted on the relaxed ground state geometries. The simulated spectra, along with the band assignments, have been compiled in the ESI (Table S2 and Fig. S32†). It should be noted that the simulated spectra match well the experimental trends.

The primary transition is a mixture of MLCT and LLCT (L = phenylbenzimidazole) in all complexes except for IrL^6_2 and IrL^8_2. Additionally, all complexes exhibit a weak initial transition (with a small oscillator strength) that corresponds to ML′CT and LL′CT (charge towards the picolinate moieties), except for IrL^7_2 and IrL^{10}_2 which exhibit two rather strong transitions that are close in energy. IrL^5_2 is the only complex that

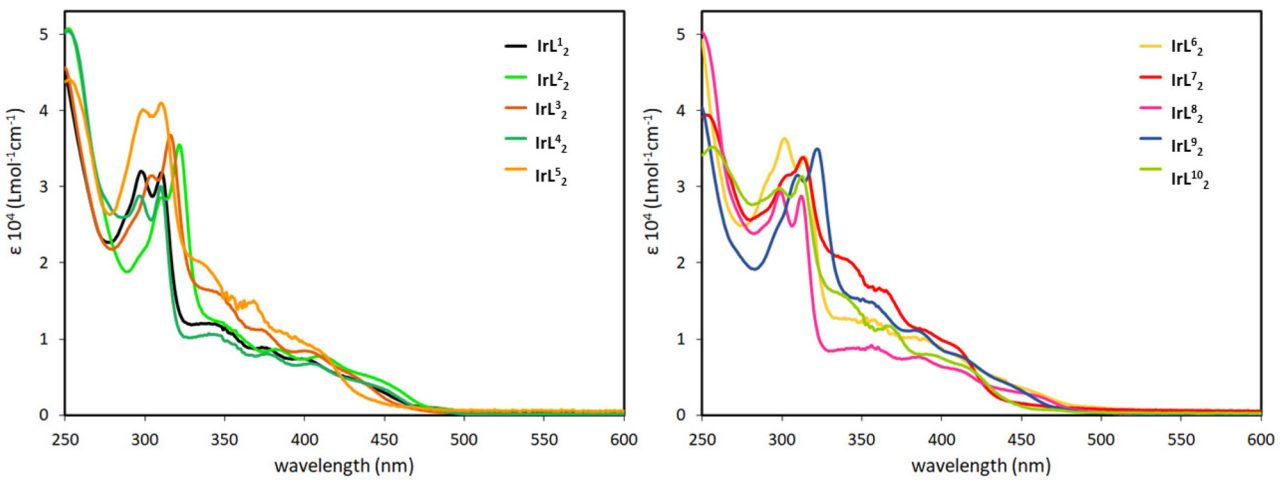

Fig. 2 Absorption spectra of the ten complexes in CH_2Cl_2 at room temperature.

Table 3 Photophysical properties

	Photoluminescence in dilute solution of CH_2Cl_2, 298 K[a,b]							Photoluminescence at 77 K[c]	
Complex	Absorption λ [nm] ($\varepsilon \times 10^3$ [M^{-1} cm^{-1}])	λ [nm]	Φ (air)	τ [μs] (air)	$k_r \times 10^5$ [s^{-1}]	$k_{nr} \times 10^5$ [s^{-1}]	$k[O_2]^d \times 10^9$ [M^{-1} s^{-1}]	E^{00} [e] (eV)	λ [nm]	τ [μs]
$\mathbf{IrL^1}_2$	298 (31.9), 310 (31.8), 345 (11.9), 375 (8.8), 402 (7.3), 429 (4.8), 480 (1.0)	503, 537[f]	0.09 (0.02)	0.32 (0.08)	2.8	28.4	5.0	2.47	486[f], 521, 567	3.31
$\mathbf{IrL^2}_2$	309 (28.3), 322 (35.4), 350 (11.8), 382 (8.2), 413 (7.7), 441 (5.1), 488 (0.8)	507[f], 542, 587sh	0.35 (0.03)	1.10 (0.12)	3.5	5.9	4.4	2.45	490[f], 530, 573, 627sh	2.94
$\mathbf{IrL^3}_2$	304 (31.4), 316 (36.7), 347 (15.8), 374 (11.1), 403 (8.4), 431 (5.1), 493 (0.3)	516, 552[f], 600sh	0.11 (0.01)	0.89 (0.10)	1.2	10.0	5.1	2.40	500[f], 537, 584, 640sh	4.10
$\mathbf{IrL^4}_2$	297 (28.8), 309 (29.7), 343 (10.7), 376 (8.4), 408 (6.7), 442 (3.5), 484 (0.7)	502[f], 532, 580sh	0.42 (0.03)	1.21 (0.12)	3.5	4.8	4.9	2.47	488[f], 521, 563, 616sh	3.49
$\mathbf{IrL^5}_2$	299 (40.1), 311 (40.8), 336 (20.0), 369 (14.7), 410 (8.4), 468 (1.1)	563	0.04 (0.01)	0.32 (0.08)	1.2	30.0	4.3	2.20	471, 507[f], 547	4.58
$\mathbf{IrL^6}_2$	302 (36.3), 314 (33.9), 357 (12.5), 387 (9.9), 408 (7.7), 449 (3.7), 496 (1.0)	514[f], 554, 605sh	0.40 (0.03)	1.02 (0.19)	3.9	5.9	5.5	2.41	505[f], 544, 589	4.40
$\mathbf{IrL^7}_2$	302 (30.8), 313 (33.3), 341 (19.9), 362 (15.9), 389 (10.7), 410 (8.4), 457 (0.8)	500sh, 560[f]	0.30 (0.04)	1.07 (0.19)	2.8	6.5	2.8	2.48	486[f], 526, 569, 621sh	6.75
$\mathbf{IrL^8}_2$	298 (29.4), 312 (28.7), 358 (8.8), 387 (7.6), 412 (5.8), 462 (2.3), 491 (0.6)	516[f], 554, 600sh	0.43 (0.05)	1.91 (0.23)	2.2	3.0	1.8	2.40	500[f], 541, 584	4.31
$\mathbf{IrL^9}_2$	309 (31.9), 322 (35.0), 356 (14.9), 384 (11.2), 412 (7.8), 446 (3.7), 491 (0.4)	485, 519[f], 554sh	0.17 (0.02)	0.78 (0.10)	2.2	10.6	4.4	2.56	470[f], 506, 544	3.35
$\mathbf{IrL^{10}}_2$	299 (29.7), 313 (30.8), 337 (15.8), 367 (11.7), 395 (7.9), 416 (6.3), 472 (0.6)	536[f], 578, 627sh	0.24 (0.03)	0.91 (0.08)	2.6	8.3	3.5	2.31	519[f], 562, 612	4.04

[a] $Ir(ppy)_3$ in CH_2Cl_2 was used as a reference. [b] In deaerated solution unless otherwise mentioned. [c] Recorded in butyronitrile. [d] With $[O_2] = 2.2$ mM in dichloromethane. [e] Energy of the emitting excited state. [f] The most intense band.

exhibits two very weak transitions corresponding to ML′CT and LL′CT before the primary transition (MLCT and LLCT). Moreover, this strong transition is approximately 0.20 eV higher in energy than in the other complexes. Complex $\mathbf{IrL^7}_2$ also exhibits such a pattern. These differences compared to other complexes may explain a distinct excited state energy order for these complexes.

Emission spectroscopy. The emission spectra of the complexes have been recorded in both deaerated and air-equilibrated dilute solution of CH_2Cl_2 at room temperature and at 77 K in butyronitrile rigid matrix. The room temperature spectra are displayed in Fig. 3. The photophysical data are gathered in Table 3 and the individual spectra are to be found in ESI† as well as those at 77 K. At r.t., the complexes display structured emission spectra (with the exception of $\mathbf{IrL^5}_2$ and $\mathbf{IrL^7}_2$ whose emission spectra are broad) in the visible range, with lifetimes of μs, with large Stokes shifts, and sensitivity to the presence of oxygen ($k[O_2]$ ranging from 1.8 M^{-1} s^{-1} to 5.5 M^{-1} s^{-1}). Therefore the emission can be ascribed to phosphorescence as expected for this family of iridium(III) complexes. The photoluminescence quantum yields range from 0.04 to 0.43 in deaerated CH_2Cl_2. The photophysical properties of $(ppy)_2Irpic$[77] are worth comparing with those of $\mathbf{IrL^1}_2$. $(ppy)_2Irpic$ displays an emission at 505 nm ($\Phi = 0.15$, $\tau = 514$ ns, deaerated) in CH_2Cl_2 which is comparable with $\mathbf{IrL^1}_2$, but the use of 2-phenylbenzimidazole instead of 2-phenylpyridine as cyclometallating ligand seems to induce a broadening of the emission band with a concomitant more pronounced vibronic progression.[77] Albeit, in both complexes the nature of the emitting excited state is predominantly ^{3}IL, in view of the slight rigidochromism (~10 nm) observed at low temperature.

The introduction of electron withdrawing group solely (*i.e.* CF3 and Cl) either on the benzimidazole ($\mathbf{IrL^2}_2$ and $\mathbf{IrL^4}_2$) or on the cyclometallating ring ($\mathbf{IrL^6}_2$) does not induce a pronounced hypsochromic shift in comparison with $\mathbf{IrL^1}_2$. As a consequence, $\mathbf{IrL^4}_2$ and $\mathbf{IrL^2}_2$ display emission spectra in the same range as $\mathbf{IrL^1}_2$, whereas $\mathbf{IrL^6}_2$ displays a slight bathochromic shift ($E^{00} = 2.20$ eV). Along these four complexes the shape of the spectra changes by getting more structured, which is accompanied by an increase of k_r (*i.e.* radiative rate constant) from 2.8×10^5 s^{-1} to 3.9×10^5 s^{-1} for $\mathbf{IrL^1}_2$ and $\mathbf{IrL^6}_2$ respectively. On the other hand, the introduction of electron donating group solely on either the benzimidazole ($\mathbf{IrL^3}_2$) or the cyclometallating ring ($\mathbf{IrL^5}_2$) induces a slight bathochromic shift in comparison with $\mathbf{IrL^1}_2$, with E^{00} of 2.47 eV, 2.40 eV and 2.20 eV for $\mathbf{IrL^1}_2$, $\mathbf{IrL^3}_2$, and $\mathbf{IrL^5}_2$ respectively. The k_r is 1.2×10^5 s^{-1} for both $\mathbf{IrL^3}_2$ and $\mathbf{IrL^5}_2$, smaller than k_r (2.8×10^5 s^{-1}) observed for $\mathbf{IrL^1}_2$ and, in addition, $\mathbf{IrL^5}_2$ displays a broad emission.

The substitution by electron withdrawing ($\mathbf{IrL^8}_2$) or by electron donating ($\mathbf{IrL^7}_2$) groups on both "sides" of the 2-phenylbenzimidazole does induce slight changes in the emission energy. The presence of two CF_3 groups in $\mathbf{IrL^8}_2$ draws a hypsochromic shift of the emission (in accordance with the E^{00} of 2.40 eV) and the radiative rate constant decreases slightly (2.2×10^5 s^{-1}), in comparison with $\mathbf{IrL^1}_2$. On the other hand, a similar substitution by MeO groups for $\mathbf{IrL^7}_2$ has quite a

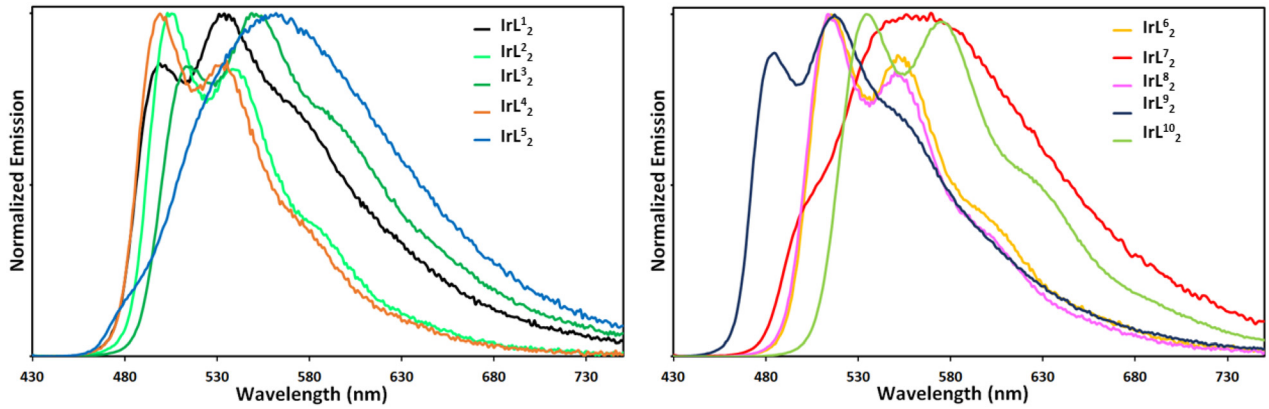

Fig. 3 Emission spectra of the ten complexes in dilute solution of CH_2Cl_2 at room temperature.

dramatic consequence on the emission spectrum shape, which becomes structureless and displays a bathochromic shift with E^{00} of 2.21 eV. One can notice that k_r are similar for these two complexes, 2.8×10^5 s^{-1}. Finally, the last two position isomers, **IrL^9$_2$** and **IrL^{10}$_2$**, substituted by antagonist functional groups in different positions, CF_3 and OMe, exhibit distinct emission spectra. Both spectra are structured with similar radiative constants, 2.2×10^5 s^{-1} and 2.6×10^5 s^{-1}, respectively, for **IrL^9$_2$** and **IrL^{10}$_2$**, that are less than that observed for **IrL^1$_2$** ($k_r = 2.8 \times 10^5$ s^{-1}), particularly for **IrL^9$_2$**. The impact of the position of the substituent is dramatic when looking at the emission energy: while **IrL^9$_2$** displays a hypsochromic shift, with E^{00} of 2.56 eV, the **IrL^{10}$_2$** spectrum is red shifted, with E^{00} of 2.31 eV, both with respect to **IrL^1$_2$** (2.47 eV).

The ^{3}MLCT or ^{3}LC nature of the phosphorescence-emitting excited states can be experimentally assessed by the photophysical properties.[37,78] For instance, a typical ^{3}MLCT emission like that of *fac*-Ir(ppy)$_3$ will display a radiative constant of around 2×10^5 s^{-1} ($\tau \sim 2$ μs), and for the case of a pure ^{3}LC emission the radiative constant will be smaller, like that of (thpy)$_2$Ir(acac)[79] (thpy = 2-(2-pyridyl)benzothiophene; acac = acetylacetonate) which displays a k_r of 0.2×10^5 s^{-1} ($\tau \sim 5.3$ μs). Within the series, the radiative constants range from 1.2×10^5 s^{-1} to 3.9×10^5 s^{-1}, which seems to indicate that most of the complexes display an emission emanating from the radiative deactivation of a lowest ^{3}MLCT state, with the exception of **IrL^3$_2$** and **IrL^5$_2$**, whose radiative constants are significantly lower than 2×10^5 s^{-1}. However, k_r is not the only parameter that allows one to characterize the nature of the lowest excited state and other experimental parameters have to be considered: (i) the shape of the emission spectrum which is structureless and broad for an emission emanating from a ^{3}MLCT, (ii) the rigidochromic effect at low temperature, and (iii) the linear relationship[80] for ^{3}MLCT emission between the emission energy and $\Delta E_{1/2} = (E_{ox} - E_{red})$ eV. Thus, with regard to the shape of the spectrum, only **IrL^5$_2$** and **IrL^7$_2$** display a broad and structureless emission which is characteristic of a ^{3}MLCT emission. The rigidochromism is a property of the transition metal complexes with an emission emanating from the radiative deactivation of ^{3}CT excited state, typically ^{3}MLCT, displaying a blue-shifted emission when the solution environment becomes rigid, by lowering the temperature in solution.[33] The superimposed spectra at r.t. and in benzonitrile at 77 K are presented in Fig. S4.† Looking at the spectra, two features are observed, being a marked rigidochromism and a slight one.

Complexes **IrL^5$_2$** and **IrL^6$_2$** are very representative and the superimposed spectra are shown in Fig. 4. It is somewhat striking that the emission spectra at r.t. in CH_2Cl_2 and at 77 K in butyronitrile are almost superimposed for **IrL^6$_2$**. Within the series, only **IrL^5$_2$** and **IrL^7$_2$** exhibit broad emission spectra at r.t., displaying a strong rigidochromic effect and a change in the spectra shape. Finally, a linear relation between the emission energy and $\Delta E_{1/2}$ is not verified within the series, which rules out an emission emanating from the pure ^{3}MLCT for this family of complexes. To conclude, while the excited states (^{3}IL, ^{3}ILCT and ^{3}MLCT) are known to be very close in iridium(III) complexes, it seems that, in the light of the experimental results, the present series of complexes displays an emission at r.t. with a strong proportion of ^{3}IL excited state, with the exception of **IrL^5$_2$** and **IrL^7$_2$**, whose emission at r.t. has strong ^{3}MLCT character. As the primary transition is a mixture of MLCT and LLCT (see above), the complexes rapidly undergo intersystem crossing and the ^{3}MLCT and ^{3}ILCT are populated and a subsequent internal conversion leads to the population of the ^{3}IL excited state.

To gain a deeper understanding of the phosphorescence properties, we performed optimizations of the first triplet excited state and simulations of the luminescence resulting from this state. As shown in Fig. S33 of the ESI,† our simulated spectra match the recorded spectra at room temperature. The relative intensities and peak positions are well reproduced in our simulations, and we accurately replicate the spacing between the peaks in cases where there is sufficient vibronic coupling. Additionally, our simulations capture the bell-curve shape observed in the luminescence spectra of **IrL^5$_2$** and **IrL^7$_2$**, further validating our model. The correlation between the simulated and observed luminescence at room temperature is shown in Fig. S34.† This high level of agreement allows us to

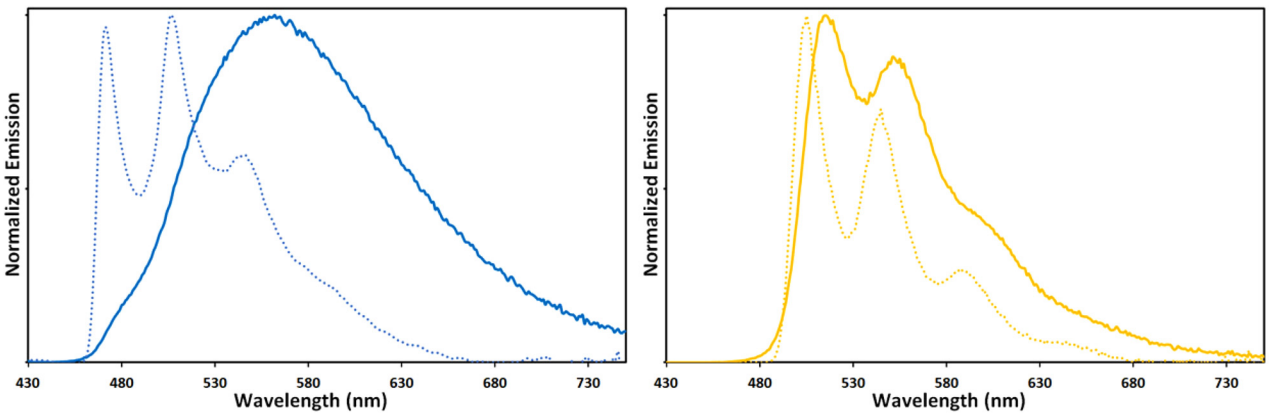

Fig. 4 Superimposition of the emission spectra at room temperature (full line) in CH_2Cl_2 and at 77 K (dashed line) in butyronitrile of complexes IrL^5_2 (left) and IrL^6_2 (right).

confidently localize the electrons in the excited state (spin density) and estimate the expected colour using a CIE (x,y) horseshoe diagram. Most of the complexes have a spin density localized over the metal and phenylbenzimidazole moieties (Fig. S35†). However, for IrL^5_2 and, surprisingly, IrL^9_2, the spin density is localized on the metal and the picolinate moieties, with a larger spin density on the picolinate for IrL^5_2 than for IrL^9_2. These findings explain the distinctive behaviour of complex IrL^5_2 compared to the others. Finally, we can compare the predicted colours from our simulations with the observed ones, as shown in Fig. 5. As one can see, our simulations reproduce well the observed colour.

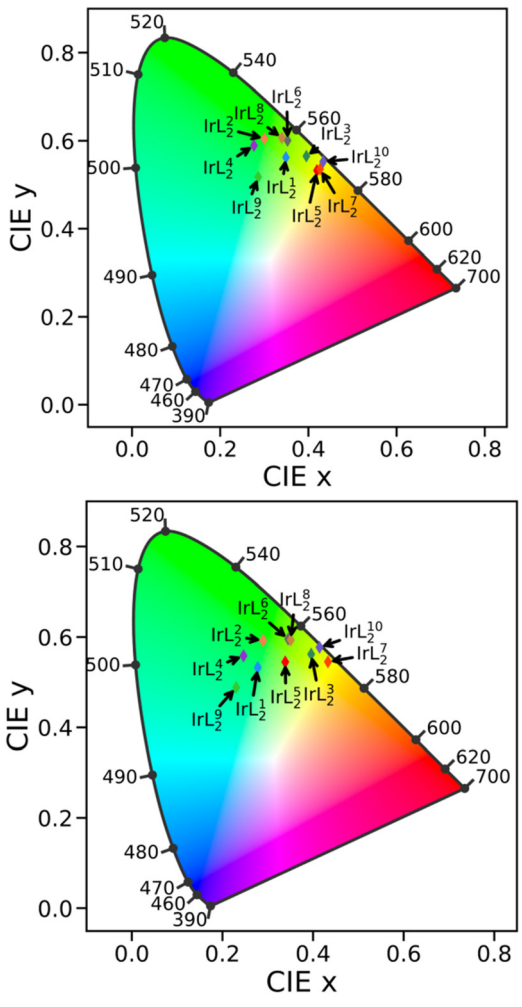

Fig. 5 Chromaticity diagram CIE-1931: experimental (top) and simulated (bottom) color.

Conclusion

We described a series of ten original 2-phenylbenzimidazole-based iridium(III) complexes with picolinate ancillary ligand, which have been characterized by NMR, HRMS and elemental analysis. Their luminescence properties have been studied in dilute solution at room temperature and in butyronitrile at low temperature, both in steady state and in time resolved spectroscopy. We demonstrated that the choice of the substituent on the cyclometallating ligand allows one to finely tune the emission energy of the complexes by manipulating the electronic properties (*i.e.* Hammett parameter), which also has an influence on the electrochemical properties. Moreover, the nature of the lowest-lying excited state(s) is affected by the substituents and their position, and the emission emanates from the radiative deactivation of ^{3}CT or ^{3}IL excited states. In particular IrL^5_2 can be recognized as a "genuine" ^{3}MLCT emitter whereas IrL^6_2 displays the opposite behaviour being a "true" ^{3}IL emitter, which has been demonstrated by both experimental techniques and state-of-the-art computational methods.

Experimental

Synthesis of the complexes

The crude μ-dichloridodimers were synthetized from HL^1–HL^{10} and $IrCl_3{\cdot}nH_2O$ as reported in our previous work.[59] In a round-bottom flask under argon, the selected μ-dichloridodi-

mer, 2-picolinic acid and Na_2CO_3 (1 : 3 : 3) were dissolved in a deaerated 3 : 1 mixture of 2-ethoxyethanol/water and heated at 100 °C overnight. At r.t., water was added, and the precipitate was filtered off, washed with water and diethylether, and dried. The precipitates were purified over pre-treated SiO_2 with Et_3N using CH_2Cl_2/CH_3OH as eluent.

IrL$^1_2$. Crude $[Ir(L^1)_2(\mu\text{-Cl})]_2$ (0.041 g, 0.06 mmol), 2-picolinic acid (0.022 g, 0.18 mmol), Na_2CO_3 (0.19 g, 0.18 mmol) and 2-ethoxyethanol/water 3 : 1 (10 mL). SiO_2 (CH_2Cl_2/CH_3OH 9 : 1). Product isolated as yellow powder (41 mg, 89%). ^{1}H NMR (500 MHz, CD_2Cl_2) δ 8.15–8.11 (m, 1H; H_α), 7.99 (dd, J = 8.0, 0.6 Hz, 1H; H_{10}), 7.88–7.86 (m, 2H; $H_{\beta,\,\delta}$), 7.79 (d, J = 9.0 Hz, 1H; $H_{5'}$), 7.77 (d, J = 9.1 Hz, 1H; H_5), 7.70 (d, J = 8.4 Hz, 1H; $H_{13'}$), 7.68 (d, J = 7.9 Hz, 1H; H_{13}), 7.32 (td, J = 7.0, 1.5 Hz, 1H; H_γ), 7.31–7.27 (m, 1H, H_{12}), 7.27–7.23 (m, 1H; H_{11}), 7.21 (ddd, J = 8.3, 7.3, 1.0 Hz, 1H, $H_{12'}$), 6.96 (dt, J = 15.2, 7.6 Hz, 2H, $H_{4',\,4}$), 6.86 (ddd, J = 8.2, 7.4, 0.9 Hz, 1H; $H_{11'}$), 6.70 (tdd, J = 7.5, 3.4, 1.2 Hz, 2H; $H_{3',\,3}$), 6.51 (dd, J = 7.7, 0.9 Hz, 1H; $H_{2'}$), 6.22 (dd, J = 7.7, 0.9 Hz, 1H; H_2), 5.80–5.67 (m, 3H; H_{10}, 2($CH(CH_3)_2$)), 1.86 (ddd, J = 9.8, 6.9, 4.9 Hz, 12H; 2($CH(CH_3)_2$)). ^{13}C NMR (126 MHz, CD_2Cl_2) δ 173.4, 164.1, 163.1, 154.0, 152.6, 150.5, 149.8, 141.3, 141.2, 137.8, 136.0, 135.54, 135.46, 134.7, 134.2, 133.9, 129.9, 129.6, 128.1, 127.8, 125.7, 125.4, 124.3, 123.7, 123.1, 122.6, 121.7, 121.1, 117.9, 115.2, 114.3, 113.7, 50.3, 50.3, 22.1, 22.1, 21.9, 21.8. HRMS (ESI) found m/z 786.24064, calcd m/z 786.24166 for $C_{38}H_{35}IrN_5O_2$ $[M\text{-}H]^+$. Elemental analysis calcd (%) for $C_{38}H_{34}IrN_5O_2{\cdot}CH_3OH$, C, 57.34; H, 4.69; N, 8.57, found C, 57.09; H, 4.74; N, 8.51.

IrL$^2_2$. Crude $[Ir(L^2)_2(\mu\text{-Cl})]_2$ (0.050 g, 0.06 mmol), 2-picolinic acid (0.022 g, 0.18 mmol), Na_2CO_3 (0.019 g, 0.18 mmol) and 2-ethoxyethanol/water 3 : 1 (10 mL). Purification over SiO_2 was not possible due to the low solubility of the complex. The complex was washed with H_2O, diethylether and methanol, then recrystallized in a CH_2Cl_2/pentane mixture. The product was isolated as a pale-yellow powder (52 mg, 95%). ^{1}H NMR (500 MHz, CD_2Cl_2) δ 8.19 (dd, J = 7.8, 0.5 Hz, 1H; H_α), 8.14 (s, 1H; H_{10}), 7.95 (td, J = 7.7, 1.6 Hz, 1H; H_β), 7.85–7.82 (m, 1H; H_δ), 7.80–7.78 (m, 3H, $H_{13,\,13'}$, H_5), 7.77 (d, J = 7.9 Hz, 1H, $H_{5'}$), 7.40 (ddd, J = 7.5, 5.4, 1.5 Hz, 1H; H_γ), 7.03–6.946 (m, 2H; $H_{4',\,4}$), 6.78–6.72 (m, 2H; $H_{3',\,3}$), 6.51 (dd, J = 7.7, 0.8 Hz, 1H; $H_{2'}$), 6.20 (dd, J = 7.7, 0.8 Hz, 1H; H_2), 5.69 (dh, J = 14.1, 6.9 Hz, 2H; 2($CH(CH_3)_2$)), 5.58 (s, 1H, $H_{10'}$), 1.87–1.78 (m, 12H, 2($CH(CH_3)_2$)). ^{13}C NMR (126 MHz, CD_2Cl_2) δ 173.2, 166.3, 165.2, 153.9, 152.7, 150.9, 149.9, 140.6, 140.4, 138.4, 135.6, 135.5, 134.7, 134.6, 133.4, 133.1, 130.7, 130.3, 128.6, 128.3, 128.2, 127.9, 127.1, 126.4, 126.2, 125.9, 122.1, 121.5, 118.8, 116.3, 115.3, 115.0, 54.0, 50.8, 50.8, 22.1, 22.0, 21.9, 21.8. HRMS (ESI) found m/z 922.08386, calcd m/z 922.08545 for $C_{38}H_{31}Cl_4IrN_5O_2$ $[M - H]^+$. Elemental analysis calcd (%) for $C_{38}H_{30}Cl_4IrN_5O_2$, C, 49.46; H, 3.28; N, 7.59, found C, 49.54; H, 3.51; N, 7.62.

IrL$^3_2$. Crude $[Ir(L^3)_2(\mu\text{-Cl})]_2$ (0.054 g, 0.06 mmol), 2-picolinic acid (0.024 g, 0.19 mmol), Na_2CO_3 (0.020 g, 0.19 mmol) and 2-ethoxyethanol/water 3 : 1 (10 mL). SiO_2 (CH_2Cl_2/CH_3OH) progressive increase of CH_3OH from 1% to 6.5%. Product isolated as a yellow powder (46 mg, 78%). ^{1}H NMR (500 MHz, CD_2Cl_2) δ 8.39 (s, 1H; H_{10}), 8.17 (d, J = 7.7 Hz, 1H; H_α), 7.95–7.87 (m, 2H; $H_{\beta,\,\delta}$) 7.87–7.75 (m, 4H; $H_{13',\,13}$, $H_{5',\,5}$), 7.54 (d, J = 8.4 Hz, 1H; H_{12}), 7.45 (d, J = 8.6 Hz, 1H; H_{12}), 7.41–7.35 (m, 1H; H_γ), 7.05–6.95 (m, 2H; $H_{4',\,4}$), 6.75 (dd, J = 14.0, 6.9 Hz, 2H; $H_{3',\,3}$), 6.55 (d, J = 7.6 Hz, 1H; H_2), 6.23 (d, J = 7.6 Hz, 1H; H_2), 5.82 (s, 1H; $H_{10'}$) 5.81–5.71 (m, 2H; 2($CH(CH_3)_2$)), 2.02–1.73 (m, J = 6.6 Hz, 12H; 2($CH(CH_3)_2$)). ^{13}C NMR (126 MHz, CD_2Cl_2) δ 173.1, 166.4, 165.3, 154.0, 152.9, 151.2, 149.9, 140.9, 140.6, 138.3, 136.2, 136.0, 135.7, 135.2, 134.7, 130.7, 130.3, 128.24, 128.19, 128.16, 126.6, 126.4, 126.3, 126.12, 126.07, 126.0, 126.0, 125.8, 125.7, 123.9, 123.7, 122.0, 121.5, 120.00, 119.97, 119.9, 119.5, 119.4, 119.4, 115.52, 115.49, 115.45, 115.42, 114.7, 114.3, 112.71, 112.68, 112.64, 112.60, 50.81, 50.77, 22.15, 22.07, 22.0, 21.9. ^{19}F NMR (470 MHz, CD_2Cl_2) δ −61.2, −61.5. HRMS (ESI) found m/z 922.21578, calcd m/z 922.21645 for $C_{40}H_{33}F_6IrN_5O_2$ $[M]^+$. Elemental analysis calcd (%) for $C_{40}H_{32}F_6IrN_5O_2$, C, 52.16; H, 3.51; N, 7.61, found C, 51.92; H, 3.65; N, 7.75.

IrL$^4_2$. Crude $[Ir(L^4)_2(\mu\text{-Cl})]_2$ (0.067 g, 0.09 mmol), 2-picolinic acid (0.032 g, 0.27 mmol), Na_2CO_3 (0.028 g, 0.27 mmol) and 2-ethoxyethanol/water 3 : 1 (10 mL). SiO_2 (CH_2Cl_2/CH_3OH) progressive increase of CH_3OH until 5%. Product isolated as a yellow-orange powder (57 mg, 76%). ^{1}H NMR (500 MHz, CD_2Cl_2) δ 8.15–8.11 (m, 1H; H_α), 7.90–7.83 (m, 3H; H_{10}, $H_{\beta,\,\delta}$), 7.73 (d, J = 8.1 Hz, 1H; H_5), 7.71 (d, J = 8.1 Hz, 1H; $H_{5'}$), 7.32 (dd, J = 5.6, 1.6 Hz, 1H, H_γ), 7.15 (d, J = 2.3 Hz, 1H; $H_{13'}$), 7.12 (d, J = 2.2 Hz, 1H, H_{13}), 6.98–6.88 (m, 3H; H_{11}, $H_{4',\,4}$), 6.71–6.65 (m, 2H; $H_{3',\,3}$), 6.50 (dd, J = 9.0, 2.4 Hz, 1H; $H_{11'}$), 6.48 (dd, J = 7.7, 1.0 Hz, 1H; $H_{2'}$), 6.21 (dd, J = 7.7, 0.9 Hz, 1H; H_2), 5.69 (pd, J = 13.2, 6.3 Hz, 2H; 2($CH(CH_3)_2$)), 5.56 (d, J = 9.0 Hz, 1H; $H_{10'}$), 3.86 (s, 3H; –OCH_3), 3.83 (s, 3H; –OCH_3), 1.88–1.79 (m, 12H; 2($CH(CH_3)_2$)). ^{13}C NMR (126 MHz, CD_2Cl_2) δ 173.35, 163.58, 162.46, 156.79, 156.33, 154.00, 152.02, 149.79, 137.76, 136.33, 135.89, 135.77, 135.72, 135.28, 134.88, 134.62, 129.51, 129.19, 128.00, 127.73, 125.18, 124.95, 121.57, 120.98, 118.38, 115.68, 112.60, 112.19, 98.50, 98.19, 56.51, 56.48, 50.07, 21.85, 21.84, 21.72, 21.63. HRMS (ESI) found m/z 846.26208, calcd m/z 846.26281 for $C_{40}H_{39}IrN_5O_4$ $[M - H]^+$. Elemental analysis calcd (%) for $C_{40}H_{38}IrN_5O_4{\cdot}H_2O$, C, 55.67; H, 4.67; N, 8.12, found C, 55.81; H, 4.75; N 7.98.

IrL$^5_2$. Crude $[Ir(L^5)_2(\mu\text{-Cl})]_2$ (0.049 g, 0.06 mmol), 2-picolinic acid (0.022 g, 0.18 mmol), Na_2CO_3 (0.019 g, 0.18 mmol) and 2-ethoxyethanol/water 3 : 1 (10 mL). SiO_2 (CH_2Cl_2/CH_3OH/Et_3N) progressive increase of CH_3OH from 1% to 6.5%. Product isolated as a bright yellow powder (29 mg, 54%). ^{1}H NMR (500 MHz, CD_2Cl_2) δ 8.17 (dd, J = 7.8, 0.5 Hz, 1H; H_α), 8.02 (d, J = 8.0 Hz, 1H; H_{10}), 7.91 (td, J = 7.7, 1.5 Hz, 1H; H_β), 7.88–7.78 (m, 3H; H_δ, $H_{5,5'}$), 7.76 (d, J = 8.4 Hz, 1H; H_{13}), 7.73 (d, J = 8.3 Hz, 1H; $H_{13'}$), 7.40–7.35 (m, 2H; H_γ,H_{12}), 7.30 (ddd, J = 16.7, 8.3, 1.0 Hz, 2H; $H_{12'}$, H_{11}), 7.23 (dd, J = 8.3, 1.3 Hz, 1H; $H_{4'}$), 7.18 (dd, J = 8.3, 1.3 Hz, 1H; H_4), 6.94 (t, J = 7.8 Hz, 1H; $H_{11'}$), 6.62 (d, J = 1.4 Hz, 1H; $H_{2'}$), 6.30 (d, J = 1.4 Hz, 1H; H_2), 5.78–6.54 (m, 3H; 2($CH(CH_3)_2$), H_{10}), 1.90 (dd, J = 9.5, 7.0 Hz, 3H; $CH(CH_3)_2$), 1.83 (t, J = 6.9 Hz, 3H; $CH(CH_3)_2$).^{13}C NMR (126 MHz, CD_2Cl_2) δ 173.4, 162.8, 161.9, 153.7, 152.2, 150.5, 149.9, 141.0, 140.9, 139.73, 139.72, 139.44, 139.43, 138.41, 134.1, 133.9, 130.80, 130.78, 130.75, 130.6, 130.3, 130.13, 130.10, 130.08, 128.4, 128.0, 125.53, 125.49, 125.3, 125.2,

125.1, 124.4, 124.1, 123.6, 123.3, 123.2, 118.9, 118.84, 118.81, 118.30, 118.27, 118.24, 118.1, 115.4, 114.6, 114.0, 50.78, 50.77, 22.00, 21.96, 21.9, 21.8. ^{19}F NMR (470 MHz, CD_2Cl_2) δ −63.3, −63.5. HRMS (ESI) found *m/z* 922.21583, calcd *m/z* 922.21645 for $C_{40}H_{33}F_6IrN_5O_2$ $[M\text{-}H]^+$. Elemental analysis calcd (%) for $C_{40}H_{32}F_6IrN_5O_2{\cdot}H_2O$, C, 51.17; H, 3.65; N, 7.46, found C, 51.28; H, 3.76; N, 7.31.

IrL$^6_2$. Crude $[Ir(\mathbf{L^6})_2(\mu\text{-Cl})]_2$ (0.052 g, 0.07 mmol), 2-picolinic acid (0.025 g, 0.20 mmol), Na_2CO_3 (0.022 g, 0.020 mmol) and 2-ethoxyethanol/water 3 : 1 (10 mL). SiO_2 (CH_2Cl_2/CH_3OH) progressive increase of CH_3OH until 5%. Product isolated as an orange-yellowish powder (29 mg, 49%). ^{1}H NMR (500 MHz, CD_2Cl_2) δ 8.14 (d, J = 7.4 Hz, 1H; H_α), 8.00–7.94 (m, 1H; H_β), 7.90 (d, J = 5.3 Hz, 1H; H_{10}), 7.87 (td, J = 7.7, 1.5 Hz, 1H; H_δ), 7.73 (d, J = 8.8 Hz, 1H. H_5), 7.71 (d, J = 8.8 Hz, 1H; $H_{5'}$), 7.67–7.62 (m, 2H; $H_{13,13'}$), 7.36–7.32 (m, 1H; H_γ), 7.28–7.22 (m, 2H; $H_{12,\ 11}$), 7.17 (t, J = 7.8 Hz, 1H; $H_{12'}$), 6.85 (t, J = 7.3 Hz, 1H; $H_{11'}$), 6.56 (dd, J = 8.7, 2.7 Hz, 1H; $H_{4'}$), 6.51 (dd, J = 8.7, 2.7 Hz, 1H; H_4), 5.94 (d, J = 2.6 Hz, 1H; $H_{2'}$), 5.70 (d, J = 2.7 Hz, 1H; H_2), 5.69 (d, J = 2.8 Hz, 1H; $H_{10'}$), 5.68–5.56 (m, 2H; 2(C*H*(CH_3)$_2$)), 3.40 (s, 1H; Ph-OCH_3), 3.32 (s, 1H; Ph-OCH_3), 1.93–1.71 (m, 12H; 2(CH(CH_3)$_2$)). ^{13}C NMR (126 MHz, CD_2Cl_2) δ 173.4, 164.2, 163.1, 160.7, 160.4, 155.3, 153.9, 152.9, 149.8, 141.3, 141.2, 137.8, 134.0, 133.6, 128.5, 128.2, 128.0, 127.7, 126.9, 126.6, 124.2, 123.5, 122.7, 122.2, 119.6, 118.9, 117.6, 114.9, 113.9, 113.3, 108.0, 107.1, 54.9, 54.8, 50.1, 50.0, 21.9, 21.8, 21.7. HRMS (ESI) found *m/z* 846.26255, calcd *m/z* 846.26281 for $C_{40}H_{39}IrN_5O_4$ $[M - H]^+$. Elemental analysis calcd (%) for $C_{40}H_{38}IrN_5O_4$, C, 56.85; H, 4.54; N, 8.29, found C, 56.71; H, 4.78; N, 8.44.

IrL$^7_2$. Crude $[Ir(\mathbf{L^7})_2(\mu\text{-Cl})]_2$ (0.111 g, 0.11 mmol), 2-picolinic acid (0.042 g, 0.34 mmol), Na_2CO_3 (0.036 g, 0.34 mmol) and 2-ethoxyethanol/water 3 : 1 (10 mL). SiO_2 (CH_2Cl_2/CH_3OH) progressive increase from 1% to 5% of CH_3OH. Product isolated as a bright yellow powder (90 mg, 74%). ^{1}H NMR (500 MHz, CD_2Cl_2) δ 8.41 (s, 1H; H_{10}), 8.21 (d, J = 7.7 Hz, 1H; H_α), 7.98–7.91 (m, 2H; $H_{\beta,\ \delta}$), 7.91–7.81 (m, 4H; $H_{5,5'}$, $H_{13,13'}$), 7.62 (d, J = 8.8 Hz, 1H; H_{12}), 7.52 (d, J = 8.8 Hz, 1H; $H_{12'}$), 7.47–7.40 (m, 1H; H_γ), 7.28 (d, J = 8.3 Hz, 1H; $H_{4'}$), 7.22 (d, J = 8.3 Hz, 1H; H_4), 6.68 (s, 1H; $H_{2'}$), 6.29 (s, 1H; H_2), 5.86 (s, 1H; $H_{10'}$), 5.74 (hept, J = 13.8, 6.9 Hz, 2H; 2(CH(CH_3)$_2$)), 2.04–1.75 (m, 12H; 2(CH(CH_3)$_2$)). ^{13}C NMR (126 MHz, CD_2Cl_2) δ 173.1, 165.1, 164.1, 153.6, 152.3, 151.0, 150.0, 140.6, 140.2, 138.9, 138.57, 138.56, 136.1, 135.9, 131.8, 131.5, 131.3, 131.2, 131.04, 131.02, 131.99, 130.96, 130.7, 130.5, 130.08, 130.05, 130.02, 130.00, 128.5, 128.4, 127.3, 127.0, 126.7, 126.4, 126.2, 125.8, 125.6, 125.3, 125.1, 123.7, 123.5, 123.1, 123.0, 120.95, 120.92, 120.90, 120.87, 120.39, 120.36, 120.34, 119.18, 119.15, 119.12, 118.67, 118.65, 118.62, 118.59, 115.82, 115.78, 115.75, 115.71, 115.27, 114.7, 112.91, 112.88, 112.84, 112.80, 51.30, 51.27, 22.0, 21.89, 21.86. ^{19}F NMR (470 MHz, CD_2Cl_2) δ −61.5, −61.8, −63.4, −63.6. HRMS (ESI) found *m/z* 1058.19085, calcd *m/z* 1058.19124 for $C_{42}H_{31}F_{12}IrN_5O_2$ $[M - H]^+$. Elemental analysis calcd (%) for $C_{42}H_{30}F_{12}IrN_5O_2$, C, 47.72; H, 2.89; N, 6.63, found C, 47.55; H, 2.75; N, 6.87.

IrL$^8_2$. Crude $[Ir(\mathbf{L^8})_2(\mu\text{-Cl})]_2$ (0.054 g, 0.07 mmol), 2-picolinic acid (0.024 g, 0.20 mmol), Na_2CO_3 (0.021 g, 0.20 mmol) and 2-ethoxyethanol/water 3 : 1 (10 mL). SiO_2 (CH_2Cl_2/CH_3OH) progressive increase of CH_3OH until 5%. Product isolated as an orange powder (40 mg, 67%). ^{1}H NMR (500 MHz, CD_2Cl_2) δ 8.13 (d, J = 7.6, 1H; H_α), 7.86 (ddd, J = 8.9, 7.4, 5.4 Hz, 3H; $H_{\beta,\ \delta}$,H_{10}), 7.66 (t, J = 8.3 Hz, 2H; $H_{5,\ 5'}$), 7.36–7.30 (m, 1H; H_γ), 7.11 (d, J = 2.2 Hz, 1H; H_{13}), 7.08 (d, J = 2.2 Hz, 1H; $H_{13'}$), 6.88 (dd, J = 9.0, 2.3 Hz, 1H; H_{11}), 6.53 (dd, J = 8.7, 2.7 Hz, 1H; $H_{11'}$), 6.51–6.46 (m, 2H, $H_{4',4}$), 5.92 (d, J = 2.6 Hz, 1H; $H_{2'}$), 5.69 (t, J = 5.8 Hz, 1H; H_2), 5.66–5.56 (m, 2H; 2(C*H*(CH_3)$_2$)), 5.54 (d, J = 9.0 Hz, 1H; $H_{10'}$) 3.85 (s, 3H; -OCH_3), 3.82 (s, 3H; –OCH_3), 3.42 (s, 3H; Ph-OCH_3), 3.35 (s, 3H; Ph-OCH_3), 1.87–1.75 (m, 12H; 2(CH(CH_3)$_2$)). ^{13}C NMR (126 MHz, CD_2Cl_2) δ 173.4, 163.7, 162.6, 160.4, 160.2, 156.5, 156.0, 154.7, 153.9, 152.2, 149.9, 137.7, 135.8, 134.7, 134.4, 128.9, 128.6, 128.0, 127.7, 126.4, 126.2, 119.5, 118.9, 118.0, 115.2, 112.1, 111.7, 107.7, 106.8, 98.5, 98.2, 56.50, 56.47, 55.0, 54.8, 49.9, 49.8, 21.75, 21.74, 21.6, 21.5. HRMS (ESI) found *m/z* 906.28393, calcd *m/z* 906.28397 for $C_{42}H_{43}IrN_5O_6$ $[M\text{-}H]^+$. Elemental analysis calcd (%) for $C_{42}H_{42}IrN_5O_6{\cdot}CH_3OH$, C, 55.11; H, 4.95; N, 7.47, found C, 55.23; H, 4.71; N, 7.58.

IrL$^9_2$. Crude $[Ir(\mathbf{L^9})_2(\mu\text{-Cl})]_2$ (0.044 g, 0.05 mmol), 2-picolinic acid (0.018 g, 0.14 mmol), Na_2CO_3 (0.015 g, 0.14 mmol) and 2-ethoxyethanol/water 3 : 1 (10 mL). SiO_2 (CH_2Cl_2/CH_3OH) progressive increase from 1% to 10% of CH_3OH. Product isolated as an orange powder (37 mg, 63%). ^{1}H NMR (500 MHz, CD_2Cl_2) δ 8.36 (s, J = 11.6 Hz, 1H; H_{10}), 8.17 (d, J = 7.6 Hz, 1H; H_α), 7.94 (d, J = 5.3 Hz, 1H; H_δ), 7.91 (td, J = 7.7, 1.5 Hz, 1H; H_β), 7.82–7.73 (m, 4H; $H_{5,5'}$, $H_{13,13'}$), 7.50 (dd, J = 8.7, 1.3 Hz, 1H; H_{12}), 7.44–7.36 (m, 2H; H_γ, $H_{12'}$), 6.61 (dd, J = 8.8, 2.6 Hz, 1H; $H_{4'}$), 6.56 (dd, J = 8.8, 2.6 Hz, 1H; H_4), 6.00 (d, J = 2.6 Hz, 1H; $H_{2'}$), 5.79 (s, 1H; $H_{10'}$), 5.75–5.62 (m, 3H; 2(C*H*(CH_3)$_2$), H_2), 3.45 (s, 3H), 3.37 (s, 3H), 1.88–1.81 (m, 12H). ^{13}C NMR (126 MHz, CD_2Cl_2) δ 173.1, 166.4, 165.3, 161.2, 161.0, 155.6, 153.9, 153.5, 149.9, 140.9, 140.7, 138.3, 136.1, 135.8, 128.3, 128.2, 128.1, 127.7, 127.6, 127.4, 127.3, 126.6, 126.4, 126.1, 126.0, 125.91, 125.87, 125.7, 125.5, 125.2, 124.0, 123.7, 121.8, 121.6, 119.9, 119.58, 119.56, 119.53, 119.07, 119.05, 119.02, 115.02, 114.99, 114.3, 113.9, 112.12, 112.09, 108.3, 107.4, 55.0, 54.9, 50.6, 50.5, 22.01, 21.97, 21.8, 21.7. ^{19}F NMR (470 MHz, CD_2Cl_2) δ −61.2, −61.5. HRMS (ESI) found *m/z* 982.23679, calcd *m/z* 982.23760 for $C_{42}H_{37}F_6IrN_5O_4$ $[M\text{-}H]^+$. Elemental analysis calcd (%) for $C_{42}H_{36}F_6IrN_5O_4$, C, 51.42; H, 3.71; N, 7.14, found C, 51.56; H, 3.84; N, 7.25.

IrL$^{10}_2$. Crude $[Ir(\mathbf{L^{10}})_2(\mu\text{-Cl})]_2$ (0.043 g, 0.05 mmol), 2-picolinic acid (0.018 g, 0.15 mmol), Na_2CO_3 (0.016 g, 0.15 mmol) and 2-ethoxyethanol/water 3 : 1 (10 mL). SiO_2 (CH_2Cl_2/CH_3OH) progressive increase from 1% to 5% of CH_3OH. Product isolated as a bright yellow powder (27 mg, 57%). ^{1}H NMR (500 MHz, CD_2Cl_2) δ 8.17 (d, J = 7.3 Hz, 1H; H_α), 7.94–7.86 (m, 2H; H_{10}, H_β), 7.83–7.73 (m, 3H; H_δ, $H_{5,5'}$), 7.36 (ddd, J = 7.5, 5.4, 1.5 Hz, 1H; H_γ), 7.21 (dd, J = 8.3, 1.3 Hz, 1H; $H_{4'}$), 7.18–7.11 (m, 3H; $H_{18,\ 13}$, H_4), 6.95 (dd, J = 9.1, 2.3 Hz, 1H; H_{11}), 6.60 (d, J = 1.4 Hz, 1H; $H_{2'}$), 6.56 (dd, J = 9.0, 2.3 Hz, 1H; $H_{11'}$), 6.31 (d, J = 1.3 Hz, 1H; H_2), 5.70–5.61 (m, 2H; 2 (C*H*(CH_3)$_2$)), 5.60 (d, J = 9.0 Hz, 1H; H_{10}), 3.88 (s, J = 7.6 Hz, 3H; –OCH_3), 3.85 (s, 3H; –OCH_3), 1.88 (dd, J = 14.7, 7.0 Hz, 6H

2(C*H*(CH_3)$_2$)), 1.81 (t, J = 7.1 Hz, 6H 2(C*H*(CH_3)$_2$)). ^{13}C NMR (126 MHz, CD_2Cl_2) δ 173.3, 162.2, 161.1, 157.4, 156.9, 153.7, 151.6, 149.9, 149.7, 140.0, 139.8, 139.7, 138.3, 135.5, 135.4, 135.0, 134.7, 130.62, 130.59, 130.56, 130.53, 130.4, 130.1, 130.04, 130.01, 129.98, 129.95, 129.89, 129.7, 128.3, 128.0, 125.6, 125.4, 127.0, 124.6, 123.4, 123.2, 118.78, 118.75, 118.72, 118.68, 118.22, 118.19, 118.16, 115.9, 113.7, 113.3, 98.4, 98.0, 56.5, 56.4, 50.5, 21.8, 21.70, 21.66, 21.60. ^{19}F NMR (470 MHz, CD_2Cl_2) δ −63.2, −63.3. HRMS (ESI) found m/z 982.23673, calcd m/z 982.23760 for $C_{42}H_{37}F_6IrN_5O_4$ $[M\text{-}H]^+$. Elemental analysis calcd (%) for $C_{42}H_{36}F_6IrN_5O_4$, C, 51.42; H, 3.71; N, 7.14, found C, 51.49; H, 3.37; N, 6.99.

Computational details

Density functional theory (DFT) simulations have been performed using the Gaussian16 package.[81] Based on previous theoretical investigations conducted by some of us,[82–85] we considered the B3PW91 functional[86–88] in addition to the LanL2Dz basis set, which includes a pseudopotential to describe core electrons for large atoms together with polarization functions on C (d; 0.587), N (d; 0.736), O (d; 0.961), F (d; 1.577) Cl (d; 0.75) and Ir (f; 0.938).[89–93] The polarizable continuum model (PCM)[94,95] was used to take into account solvent effects (CH_2Cl_2). For computational savings, the –OMe and –N^{i}Pr fragments were replaced by –OH and –NH groups. Geometry relaxations of the singlet (ground state) and triplet (excited state) states were performed and carefully checked by the calculation of vibrational frequencies. The general adiabatic shift approach (AS)[96] was considered for estimating vibrational contributions to the computation of emission spectra.

All the simulations of phosphorescence spectra were performed within the Franck–Condon approximation. The vibronic calculations were achieved enforcing a sum-overstates (time-independent) approach which implies a truncation of the summation over an infinite number of states. To limit the number of integrals to be taken into account, a class-based prescreening has been employed based on the work of Santoro and coworkers and as implemented in Gaussian.[97–99]

In the present work, the following parameters were enforced:

$$C_1^{\max} = 70, C_2^{\max} = 70, N_I^{\max} = 100 \times 10^8$$

The highest class state (maxbands tag) considered was 9.

Post-treatments were done using the Gaussview and VMS packages.[100–102] Horseshoe plots were realized using an in house Python code.

Conflicts of interest

There are no conflicts to declare.

Acknowledgements

The authors thank the CNRS and Université de Grenoble Alpes for their support. This work benefited from state aid managed by the National Research Agency under the "Investments for the future" and frp, the "Investissements d'avenir" program bearing the reference ANR-15-IDEX-02. E. M.-V. was supported by the CONACYT program 707986. This work was partially supported by the CBH-EUR-GS (ANR-17-EURE-0003). For the purpose of Open Access, a CC-BY 3.0 public copyright licence (https://creativecommons.org/licenses/by/3.0/) has been applied by the authors to the present document and will be applied to all subsequent versions up to the Author Accepted Manuscript arising from this submission. The NanoBio ICMG (UAR 2607) is acknowledged for providing facilities for mass spectrometry (A. Durand, L. Fort, and R. Gueret), and single-crystal X-ray diffraction (N. Altounian).

References

1 D. J. Gaspar and E. Polikarpov, *OLED Fundamentals: Materials, Devices, and Processing of Organic Light-Emitting Diodes*, CRC Press, 1st edn, 2015.
2 A. Sandström, P. Matyba and L. Edman, *Appl. Phys. Lett.*, 2010, **96**, 053303.
3 J. Kalinowski, V. Fattori, M. Cocchi and J. A. G. Williams, *Light-emitting devices based on organometallic platinum complexes as emitters*, Springer International Publishing, Berlin, Heidelberg Germany, 2011, vol. 255.
4 H. Yersin, *Topics in Current Chemistry*, 2004, pp. 1–26.
5 H. Yersin, *Highly Efficient OLEDs with Phosphorescent Materials*, Wiley, 2007.
6 M. A. Baldo, M. E. Thompson and S. R. Forrest, *Nature*, 2000, **403**, 750–753.
7 A. F. Rausch, H. H. Homeier and H. Yersin, *Organometallic Pt(II) and Ir(III) Triplet Emitters for OLED Applications and the Role of Spin–Orbit Coupling: A Study Based on High-Resolution Optical Spectroscopy*, Springer, Berlin, Heidelberg Germany, 2010.
8 C. F. R. Mackenzie, L. Zhang, D. B. Cordes, A. M. Z. Slawin, I. D. W. Samuel and E. Zysman-Colman, *Adv. Opt. Mater.*, 2023, **11**, 1–14.
9 Y. Zhang and J. Qiao, *iScience*, 2021, **24**, 102858.
10 M. Mauro, *Chem. Commun.*, 2021, **57**, 5857–5870.
11 L. F. Gildea and J. A. G. Williams, in *Organic Light-Emitting Diodes (OLEDs)*, ed. A. Buckley, Woodhead Publishing, Sawston, UK, 2013, pp. 77–113.
12 K. P. S. Zanoni, R. L. Coppo, R. C. Amaral and N. Y. Murakami Iha, *Dalton Trans.*, 2015, **44**, 14559–14573.
13 C. E. Housecroft and E. C. Constable, *Coord. Chem. Rev.*, 2017, **350**, 155–177.
14 E. Baranoff, J.-H. Yum, I. Jung, R. Vulcano, M. Grätzel and M. K. Nazeeruddin, *Chem. – Asian J.*, 2010, **5**, 496–499.
15 H. Guo, S. Ji, W. W. Wu, J. Shao and J. Zhao, *Analyst*, 2010, **135**, 2832–2840.
16 S. Medina-Rodríguez, S. A. Denisov, Y. Cudré, L. Male, M. Marín-Suárez, A. Fernández-Gutiérrez, J. F. Fernández-Sánchez, A. Tron, G. Jonusauskas, N. D. McClenaghan and E. Baranoff, *Analyst*, 2016, **141**, 3090–3097.

17 J.-L. Fillaut, J. Andriès, R. D. Marwaha, P.-H. Lanoë, O. Lohio, L. Toupet and J. A. Gareth Williams, *J. Organomet. Chem.*, 2008, **693**, 228–234.
18 P.-H. Lanoë, J.-L. Fillaut, V. Guerchais, H. Le Bozec and J. A. Gareth Williams, *Eur. J. Inorg. Chem.*, 2011, **2011**, 1255–1259.
19 E. Ortega-Forte, S. Hernández-García, G. Vigueras, P. Henarejos-Escudero, N. Cutillas, J. Ruiz and F. Gandía-Herrero, *Cell. Mol. Life Sci.*, 2022, **79**, 510.
20 J. Shen, T. W. Rees, L. Ji and H. Chao, *Coord. Chem. Rev.*, 2021, **443**, 214016.
21 C. Caporale and M. Massi, *Coord. Chem. Rev.*, 2018, **363**, 71–91.
22 C. Y.-S. Chung and V. W.-W. Yam, *Chemistry*, 2014, **20**, 13016–13027.
23 T. Tu, W. Fang, X. Bao, X. Li and K. H. Dötz, *Angew. Chem., Int. Ed.*, 2011, **50**, 6601–6605.
24 K. Li, T. Zou, Y. Chen, X. Guan and C. Che, *Chem. – Eur. J.*, 2015, 7441–7453.
25 C. K. Prier, D. A. Rankic and D. W. C. MacMillan, *Chem. Rev.*, 2013, **113**, 5322–5363.
26 H. L. B. S. Di Bella, C. Dragonetti, M. Pizzotti, D. Roberto, F. Tessore, R. Ugo, M. G. Humphrey, M. P. Cifuentes, M. Samoc, L. Murphy, J. A. G. Williams, Z. Liu, Z. Bian, C. Huang, N. C. Fletcher, M. C. Lagunas and V. Guerchais, *Top. Organomet. Chem.*, 2010, **37**, 179.
27 A. Barbieri, F. Barigelletti, E. C.-C. Cheng, L. Flamigni, T. Gunnlaugsson, R. A. G. Kirgan, D. Kumaresan, J. P. Leonard, C. B. Nolan, D. P. Rillema, C. Sabatini, R. H. Schmehl, K. Shankar, F. Stomeo, B. P. Sullivan, S. Vaidya, B. Ventura and J. A. G. Williams, Photochemistry and Photophysics of Coordination Compounds II, in *Topics in current Chemistry*, Springer, 2007.
28 D. H. Volman, G. S. Hammond, D. C. Neckers, M. Maestri, V. Balzani, C. Deuschel-Cornioley and A. Von Zelewsky, *Adv. Photochem.*, 1992, **1**, DOI: **10.1002/9780470133484.ch1**.
29 Z. Bian, M. P. Cifuentes, S. Di Bella, N. C. Fletcher, C. Dragonetti, V. Guerchais, C. Huang, M. G. Humphrey, M. C. Lagunas, J. A. G. Le Bozec, H. Williams, Z. Liu, L. Murphy, M. Pizzotti, R. M. S. Dominique, A. F. Tessore and R. Ugo, *Molecular Organometallic Materials for Optics*, Springer, 2011, vol. 33.
30 G. Lu, L. Gu, S. Li, H.-B. Han, X. Wang, C. Zhou, J.-J. Lu and L. Zhou, *New J. Chem.*, 2023, 18603–18609.
31 T. Sajoto, P. I. Djurovich, A. B. Tamayo, J. Oxgaard, W. A. Goddard and M. E. Thompson, *J. Am. Chem. Soc.*, 2009, **131**, 9813–9822.
32 P. J. Hay, *J. Phys. Chem. A*, 2002, **106**, 1634–1641.
33 A. J. Lees, *Comments Inorg. Chem.*, 1995, **17**, 319–346.
34 R. D. Costa, E. Ortí, H. J. Bolink, S. Graber, S. Schaffner, M. Neuburger, C. E. Housecroft and E. C. Constable, *Adv. Funct. Mater.*, 2009, **19**, 3456–3463.
35 A. F. Henwood and E. Zysman-Colman, *Top. Curr. Chem.*, 2016, **374**, 36.
36 L. Flamigni, A. Barbieri, C. Sabatini, B. Ventura and F. Barigelletti, *Photochemistry and Photophysics of Coordination Compounds II*, 2007, pp. 143–203.
37 P. A. Scattergood, A. M. Ranieri, L. Charalambou, A. Comia, D. A. W. Ross, C. R. Rice, S. J. O. Hardman, J.-L. Heully, I. M. Dixon, M. Massi, F. Alary and P. I. P. Elliott, *Inorg. Chem.*, 2020, **59**, 1785–1180.
38 Z.-J. Gao, T.-H. Yeh, J.-J. Xu, C.-C. Lee, A. Chowdhury, B.-C. Wang, S.-W. Liu and C.-H. Chen, *ACS Omega*, 2020, **5**, 10553–10561.
39 D. Chen, W.-Z. He, H.-S. Liao, Y.-X. Hu, D.-D. Xie, B.-Y. Wang, H.-J. Chi, Y.-L. Lv, X. Zhu and X. Li, *Org. Electron.*, 2023, **113**, 106715.
40 Z. Ge, T. Hayakawa, S. Ando, M. Ueda, T. Akiike, H. Miyamoto, T. Kajita and M. Kakimoto, *Chem. Mater.*, 2008, **20**, 2532–2537.
41 J. H. Zhao, Y. X. Hu, H. Y. Lu, Y. L. Lü and X. Li, *Org. Electron.*, 2017, **41**, 56–72.
42 J. F. Lemonnier, L. Guénée, C. Beuchat, T. A. Wesolowski, P. Mukherjee, D. H. Waldeck, K. A. Gogick, S. Petoud and C. Piguet, *J. Am. Chem. Soc.*, 2011, **133**, 16219–16234.
43 N. M. Shavaleev, S. V. Eliseeva, R. Scopelliti and J. C. G. Bünzli, *Chem. – Eur. J.*, 2009, **15**, 10790–10802.
44 J.-H. Zhao, Y.-X. Hu, Y. Dong, X. Xia, H.-J. Chi, G.-Y. Xiao, X. Li and D.-Y. Zhang, *New J. Chem.*, 2017, **41**, 1973–1979.
45 W. S. Huang, J. T. Lin, C. H. Chien, Y. T. Tao, S. S. Sun and Y. S. Wen, *Chem. Mater.*, 2004, **16**, 2480–2488.
46 J. Jayabharathi, K. Jayamoorthy and V. Thanikachalam, *J. Organomet. Chem.*, 2014, **761**, 74–83.
47 Y. Jiao, M. Li, N. Wang, T. Lu, L. Zhou, Y. Huang, Z. Lu, D. Luo and X. Pu, *J. Mater. Chem. C*, 2016, **4**, 4269–4277.
48 H. Cao, H. Sun, Y. Yin, X. Wen, G. Shan, Z. Su, R. Zhong, W. Xie, P. Li and D. Zhu, *J. Mater. Chem. C*, 2014, **2**, 2150–2159.
49 X. Wei, J. Peng, J. Cheng, M. Xie, Z. Lu, C. Li and Y. Cao, *Adv. Funct. Mater.*, 2007, **17**, 3319–3325.
50 G. Li, Y. Wu, G. Shan, W. Che, D. Zhu, B. Song, L. Yan, Z. Su and M. R. Bryce, *Chem. Commun.*, 2014, **50**, 6977–6980.
51 X. Ouyang, D. Chen, S. Zeng, X. Zhang, S. Su and Z. Ge, *J. Mater. Chem.*, 2012, **22**, 23005–23011.
52 H. T. Cao, L. Ding, J. Yu, G. G. Shan, T. Wang, H. Z. Sun, Y. Gao, W. F. Xie and Z. M. Su, *Dyes Pigm.*, 2019, **160**, 119–127.
53 J. X. Cai, T. L. Ye, X. F. Fan, C. M. Han, H. Xu, L. L. Wang, D. G. Ma, Y. Lin and P. F. Yan, *J. Mater. Chem.*, 2011, **21**, 15405–15416.
54 L. Han, D. Zhang, Y. Zhou, Y. Yang, H. Y. Woo, F. Bai and R. Yang, *Dyes Pigm.*, 2013, **99**, 1010–1015.
55 T. Yu, F. Yang, X. Chen, W. Su and Y. Zhao, *New J. Chem.*, 2017, **41**, 2046–2054.
56 H.-T. T. Mao, C.-X. X. Zang, G.-G. G. Shan, H.-Z. Z. Sun, W.-F. F. Xie and Z.-M. M. Su, *Inorg. Chem.*, 2017, **56**, 9979–9987.
57 S. V. Tatarin, P. Kalle, I. V. Taydakov, E. A. Varaksina, V. M. Korshunov and S. I. Bezzubov, *Dalton Trans.*, 2021, **50**, 6889–6900.

58 E. Martínez-Vollbert, C. Philouze, I. Gautier-Luneau, Y. Moreau, P.-H. Lanoë and F. Loiseau, *Phys. Chem. Chem. Phys.*, 2021, **23**, 24789–24800.
59 E. Martìnez-Vollbert, C. Ciambrone, W. Lafargue-Dit-Hauret, C. Latouche, F. Loiseau and P.-H. Lanoë, *Inorg. Chem.*, 2022, **61**, 3033–3049.
60 T.-R. Chen, P.-C. Liu, H.-P. Lee, F.-S. Wu and K. H.-C. Chen, *Eur. J. Inorg. Chem.*, 2017, **2017**, 2023–2031.
61 D. G. Congrave, Y. Ting Hsu, A. S. Batsanov, A. Beeby and M. R. Bryce, *Organometallics*, 2017, **36**, 981–993.
62 F. O. Garces, K. Dedeian, N. L. Keder and R. J. Watts, *Acta Crystallogr., Sect. C: Cryst. Struct. Commun.*, 1993, **49**, 1117.
63 M. Nonoyama, *Bull. Chem. Soc. Jpn.*, 1974, **47**, 767.
64 K. J. Suhr, L. D. Bastatas, Y. Shen, L. A. Mitchell, G. A. Frazier, D. W. Taylor, J. D. Slinker and B. J. Holliday, *Dalton Trans.*, 2016, **45**, 17807–17823.
65 K. J. Suhr, L. D. Bastatas, Y. Shen, L. A. Mitchell, B. J. Holliday and J. D. Slinker, *ACS Appl. Mater. Interfaces*, 2016, **8**, 8888–8892.
66 M. Martínez-Alonso, J. Cerdá, C. Momblona, A. Pertegás, J. M. Junquera-Hernández, A. Heras, A. M. Rodríguez, G. Espino, H. Bolink and E. Ortí, *Inorg. Chem.*, 2017, **56**, 10298–10310.
67 K. A. Phillips, T. M. Stonelake, K. Chen, Y. Hou, J. Zhao, S. J. Coles, P. N. Horton, S. J. Keane, E. C. Stokes, I. A. Fallis, A. J. Hallett, S. P. O'Kell, J. M. Beames and S. J. A. Pope, *Chem. – Eur. J.*, 2018, **24**, 8577–8588.
68 G. A. Jeffrey, *An Introduction to Hydrogen Bonding*, Oxford University Press, Oxford, 1997.
69 T. Steiner, *Angew. Chem., Int. Ed.*, 2002, **41**, 48–76.
70 E. Baranoff and B. F. E. Curchod, *Dalton Trans.*, 2015, **44**, 8318–8329.
71 S. Neukermans, F. Vorobjov, T. Kenis, R. De Wolf, J. Hereijgers and T. Breugelmans, *Electrochim. Acta*, 2020, **332**, 135484.
72 J. Frey, B. F. E. Curchod, R. Scopelliti, I. Tavernelli, U. Rothlisberger, M. K. Nazeeruddin and E. Baranoff, *Dalton Trans.*, 2014, **43**, 5667–5679.
73 J. C. Deaton and F. N. Castellano, *Iridium(III) in Optoelectronic and Photonics Applications*, 2017, pp. 1–69.
74 L. Silvestroni, G. Accorsi, N. Armaroli, V. Balzani, G. Bergamini, S. Campagna, F. Cardinali, C. Chiorboli, M. T. Indelli, N. A. P. Kane-Maguire, A. Listorti, F. Nastasi, F. Puntoriero and F. Scandola, *Photochemistry and Photophysics of Coordination Compounds I*, 2007, vol. 281.
75 Y. You and S. Y. Park, *Dalton Trans.*, 2009, 1267–1282.
76 G. A. Crosby, *Acc. Chem. Res.*, 1975, **8**, 231–238.
77 E. Baranoff, B. F. E. Curchod, F. Monti, F. Steimer, G. Accorsi, I. Tavernelli, U. Rothlisberger, R. Scopelliti, M. Grätzel and M. K. Nazeeruddin, *Inorg. Chem.*, 2012, **51**, 799–811.
78 A. Barbieri, F. Barigelletti, E. C.-C. Cheng, L. Flamigni, T. Gunnlaugsson, R. A. Kirgan, D. Kumaresan, J. P. Leonard, C. B. Nolan, D. P. Rillema, C. Sabatini, R. H. Schmehl, K. Shankar, F. Stomeo, B. P. Sullivan, S. Vaidya, B. Ventura, J. A. G. Williams and V. W.-W. Yam, *Topics in Current Chemistry: Photochemistry and Photophysics of Coordination Compounds II*, Springer Berlin Heidelberg, 1980, vol. 7.
79 S. Lamansky, P. Djurovich, D. Murphy, F. Abdel-Razzaq, R. Kwong, I. Tsyba, M. Bortz, B. Mui, R. Bau and M. E. Thompson, *Inorg. Chem.*, 2001, **40**, 1704–1711.
80 A. Juris, V. Balzani, F. Barigelletti, S. Campagna, P. Belser and A. von Zelewsky, *Coord. Chem. Rev.*, 1988, **84**, 85–277.
81 M. J. Frisch, G. W. Trucks, H. B. Schlegel, G. E. Scuseria, M. A. Robb, J. R. Cheeseman, G. Scalmani, V. Barone, G. A. Petersson, H. Nakatsuji, X. Li, M. Caricato, A. V. Marenich, J. Bloino, B. G. Janesko, R. Gomperts, B. Mennucci, H. P. Hratchian, J. V. Ortiz, A. F. Izmaylov, J. L. Sonnenberg, D. Williams-Young, F. Ding, F. Lipparini, F. Egidi, J. Goings, B. Peng, A. Petrone, T. Henderson, D. Ranasinghe, V. G. Zakrzewski, J. Gao, N. Rega, G. Zheng, W. Liang, M. Hada, M. Ehara, K. Toyota, R. Fukuda, J. Hasegawa, M. Ishida, T. Nakajima, Y. Honda, O. Kitao, H. Nakai, T. Vreven, K. Throssell, J. A. Jr. Montgomery, J. E. Peralta, F. Ogliaro, M. J. Bearpark, J. J. Heyd, E. N. Brothers, K. N. Kudin, V. N. Staroverov, T. A. Keith, R. Kobayashi, J. Normand, K. Raghavachari, A. P. Rendell, J. C. Burant, S. S. Iyengar, J. Tomasi, M. Cossi, J. M. Millam, M. Klene, C. Adamo, R. Cammi, J. W. Ochterski, R. L. Martin, K. Morokuma, O. Farkas, J. B. Foresman and D. J. Fox, *Gaussian 16 (Revision B.01)*, Gaussian Inc., Wallingford CT, 2016.
82 F. Vazart and C. Latouche, *Theor. Chem. Acc.*, 2015, **134**, 144.
83 C. Latouche, F. Palazzetti, D. Skouteris and V. Barone, *J. Chem. Theory Comput.*, 2014, **10**, 4565–4573.
84 C. Latouche, A. Baiardi and V. Barone, *J. Phys. Chem. B*, 2015, **119**, 7253–7257.
85 C. Latouche, D. Skouteris, F. Palazzetti and V. Barone, *J. Chem. Theory Comput.*, 2015, **11**, 3281–3289.
86 J. P. Perdew, K. Burke and Y. Wang, *Phys. Rev. B: Condens. Matter Mater. Phys.*, 1996, **54**, 16533–16539.
87 J. P. Perdew, *Phys. Rev. B: Condens. Matter Mater. Phys.*, 1986, **33**, 8822–8824.
88 A. D. Becke, *J. Chem. Phys.*, 1993, **98**, 5648–5652.
89 T. H. Dunning and P. J. Hay, *Generalized gradient approximation for the exchange-correlation hole of a many-electron system*, ed. H. F. Schaefer, Springer US, Boston, MA, 1977, pp. 1–27.
90 W. R. Wadt and P. J. Hay, *J. Chem. Phys.*, 1985, **82**, 284–298.
91 P. J. Hay and W. R. Wadt, *J. Chem. Phys.*, 1985, **82**, 299–310.
92 P. J. Hay and W. R. Wadt, *J. Chem. Phys.*, 1985, **82**, 270–283.
93 R. Schira and C. Latouche, *Dalton Trans.*, 2021, **50**, 746–753.
94 R. C. Benedetta Mennucci, *Continuum Solvation Models in Chemical Physics: From Theory to Applications*, Wiley, 2008.
95 B. Mennucci, J. Tomasi, R. Cammi, J. R. Cheeseman, M. J. Frisch, F. J. Devlin, S. Gabriel and P. J. Stephens, *J. Phys. Chem. A*, 2002, **106**, 6102–6113.
96 J. Bloino, M. Biczysko, F. Santoro and V. Barone, *J. Chem. Theory Comput.*, 2010, **6**, 1256–1274.

97 F. Santoro, R. Improta, A. Lami, J. Bloino and V. Barone, *J. Chem. Phys.*, 2007, **126**, 084509.
98 F. Santoro, A. Lami, R. Improta and V. Barone, *J. Chem. Phys.*, 2007, **126**, 184102.
99 F. Santoro, A. Lami, R. Improta, J. Bloino and V. Barone, *J. Chem. Phys.*, 2008, **128**, 224311.
100 D. Licari, A. Baiardi, M. Biczysko, F. Egidi, C. Latouche and V. Barone, *J. Comput. Chem.*, 2015, **36**, 321–334.
101 V. Barone, *Wiley Interdiscip. Rev.: Comput. Mol. Sci.*, 2016, **6**, 86–110.
102 R. Dennington, T. A. Keith and J. M. Millam, *GaussView version 6*, 2019.